Heisenberg's uncertainty relations for a hydrogen atom confined by an impenetrable spherical cavity

R. Reyes-García,[1,2,*] S. A. Cruz,[1] and R. Cabrera-Trujillo[2]

[1] *Departmento de Física, Universidad Autónoma Metropolitana-Iztapalapa, Apartado Postal 55-534, 09340 Ciudad de México, México*

[2] *Instituto de Ciencias Físicas, Universidad Nacional Autónoma de México, Apartado Postal 48-3, Cuernavaca, Morelos 62251, México*

(Received 15 April 2024; revised 26 June 2024; accepted 5 August 2024; published 15 August 2024)

The incompatibility between two observables in quantum theory is described by Heisenberg's uncertainty principle. In this work, we study spatial confinement effects on Heisenberg's uncertainty principle for a hydrogen atom located at the center of an impenetrable spherical cavity with radius r_o. Both the radial and vector representation of the uncertainty principle are considered. For this, we solve the Schrödinger equation numerically within a finite-differences approach. We find that for small cavity sizes the values of $\Delta\hat{r}\Delta\hat{p}_r$ (radial) bunch according to the number of nodes and that for Rydberg states, i.e., large excitation, they become more coherent, satisfying exactly Heisenberg's uncertainty principle, in contrast to the vector description. However, for the vector case, we find that $\Delta\hat{\mathbf{r}}$ degenerates for small cavity sizes and bunches according to the principal quantum number n for large cavities. We find that the behavior of $\Delta\hat{\mathbf{p}}$ is responsible for the breaking of the energy degeneracy for confined quantum systems. This occurs when the confinement radius is of the order of the orbital size, as determined by the electron average distance $\langle\hat{r}\rangle$. In addition, we estimate the critical cavity size for which relativistic effects become relevant and verify that the relativistic corrections to the energy, obtained from first-order perturbation theory, become important when the total energy of the atom surpasses 93.845 Hartree, corresponding to 10% of the speed of light, which is fulfilled for cavity sizes $r_o < 1$ a.u.

DOI: 10.1103/PhysRevA.110.022814

I. INTRODUCTION

Confined quantum systems have been widely studied [1–4], since they are of great importance in the development of new technologies, mainly due to the changes in their physical and chemical properties by effect of the confinement. There exist a large variety of physical systems under extreme confinement conditions, such as atoms (or molecules) trapped into fullerenes [5,6], zeolitic nanocavities [7,8], helium bubbles formed in nuclear reactor walls [9,10], atomsor ions embedded in plasma [11,12], nanowires [13,14], and quantum dots [15,16].

Many systems can be considered as low-dimensional objects [15]—for instance, graphene sheets as a two-dimensional material, nanowires as a one-dimensional one, and finally, quantum dots as a dimensionless object. Owing to the fact that these systems are located or confined in a small space region, it becomes important to determine the uncertainties in measurements of the system properties. In quantum and classical systems, the measurements of the properties of the systems, as well as the accuracy with which one can measure these properties, are important to characterize them. Unlike classical mechanics, in quantum mechanics there exist certain uncertainties when measuring physical quantities. The quantum uncertainty relations allow us to know whether two measurements related to two observable quantities are compatible or not—that is to say, the accuracy with which we are able to measure an observable without losing accuracy in the measurement of another observable. Heisenberg's uncertainty principle is a variance-based uncertainty relation for two incompatible observables A and B, related to two operators $\hat{A}$ and $\hat{B}$, respectively. This uncertainty relation has a product form [17] expressed as

$$\Delta\hat{A}^2\Delta\hat{B}^2 \geqslant \text{an irreducible lower bound.} \tag{1}$$

Some of the most important uncertainty inequalities are those corresponding to Heisenberg's uncertainty principle for position and momentum [18–20], which is a fundamental principle in quantum mechanics [21,22]. In other words, if the electrons are trapped into a small space region, and thus the value of the variance in position is small, then the variance in momentum is large, and the energy grows continuously as the available space decreases in size. Furthermore, Heisenberg's uncertainty principle has been extended to the development of quantum information science, as mentioned by Zozor *et al.* in Ref. [23]: "*...the formulation of the uncertainty principle in quantum mechanics in terms of entropic inequalities...can be considered as a generalization of Heisenberg's uncertainty principle....*" Thus, the uncertainty relations are of special interest in quantum information science for free [17,23–29] and confined systems [30–33]. Within this field of research there exist areas of knowledge such as quantum noncloning [34,35], quantum cryptography [36,37], entanglement detection [38–41], quantum spins squeezing [42–44], quantum metrology [45–47], quantum synchronization [48,49], and mixedness detection [50,51], to mention but a few.

In this work, we study a hydrogen atom confined by an impenetrable spherical cavity in order to analyze the behavior of Heisenberg's uncertainty principle under extreme conditions. The hydrogen atom, as the simplest quantum atomic system, has been useful to analyze electronic properties

*Contact author: robertjr.73@icf.unam.mx

of more complex systems under several conditions with spatial limitation [1]. In spite of the fact that there exists an exact solution for the H atom within an impenetrable spherical cavity [52,53], we focus our attention on the implementation of a finite-differences (FD) approach to solve the time-independent Schrödinger equation, since it provides a numerically efficient and accurate approach to carry out the calculations necessary for this study.

This work is organized as follows. In Sec. II, we present a summary of the system of interest as well as the important generalizations of Heisenberg's inequalities in spherical coordinates. In Sec. III, we show our results and discussion on the radial (Sec. III A) and vector (Sec. III B) representations. In Sec. III C, a first-order perturbation approach is discussed to define the critical cavity size below which relativistic effects become relevant. Finally, in Sec. IV, our conclusions are given. Our calculations are carried out within the nonrelativistic Schrödinger equation and atomic units are used all over the manuscript.

II. THEORY

A. Confined hydrogen atom by an impenetrable spherical cavity

Let us suppose that a hydrogenic atom is placed into an impenetrable spherical box, with its nuclear charge Z clamped at the center of the cavity. The cavity has a radius r_o and its center coincides with the origin of the reference frame. The Hamiltonian of the system is then given by

$$\hat{H} = -\frac{1}{2}\nabla^2 + \hat{V}(\mathbf{r}),$$
$$\hat{V}(\mathbf{r}) = \begin{cases} -\frac{Z}{r}, & r < r_o \\ \infty, & r \geqslant r_o \end{cases}. \quad (2)$$

This form of the confinement potential implies that the wave function vanishes at the boundary $r = r_o$ (Dirichlet boundary conditions).

The spherical symmetry of the potential, in Eq. (2), suggests us to write the Laplacian operator in terms of the angular momentum operator $\hat{\mathbf{L}}^2$ as

$$\nabla^2 = \frac{1}{r^2}\frac{\partial}{\partial r}\left[r^2\frac{\partial}{\partial r}\right] - \frac{1}{r^2}\hat{\mathbf{L}}^2. \quad (3)$$

The stationary Schrödinger equation associated with the Hamiltonian given by Eqs. (2) and (3) is known to be separable in its radial and angular coordinates, such that the wave function is expressed as $\psi(\mathbf{r}) = R(r)Y_\ell^m(\theta,\phi)$, with $Y_\ell^m(\theta,\phi)$ the spherical harmonics satisfying the eigenvalue equation $\hat{\mathbf{L}}^2 Y_\ell^m(\theta,\phi) = \ell(\ell+1)Y_\ell^m(\theta,\phi)$. Accordingly, the radial Schrödinger equation becomes

$$\left\{-\frac{1}{2r^2}\frac{d}{dr}\left[r^2\frac{d}{dr}\right] + \frac{\ell(\ell+1)}{2r^2} - \frac{Z}{r}\right\}R(r) = ER(r), \quad (4)$$

which may be further simplified by defining $u(r) = rR(r)$ satisfying the equation

$$-\frac{1}{2}\frac{d^2u(r)}{dr^2} + \left[\frac{\ell(\ell+1)}{2r^2} - \frac{Z}{r}\right]u(r) = Eu(r), \quad (5)$$

with the boundary conditions $u(r)|_{r=0} = u(r)|_{r=r_o} = 0$.

Equation (5) defines the eigenfunctions and eigenvalues of the hydrogen atom for the free and confined case. The only difference is caused by the boundary conditions, as discussed by Goldman *et al.* [52] and Ferreyra *et al.* [53].

B. Radial uncertainty principle

Owing to the radial symmetry of the Coulombic potential, it is convenient to resort to the radial and vector representations of Heisenberg's uncertainty inequalities when carrying out its study. We begin with the radial representation, but our generalities apply to the vector representation as well. The mentioned irreducible lower bound in Eq. (1) relies on the commutator of two operators $\hat{A}$ and $\hat{B}$, which satisfy the relation

$$[\hat{A}, \hat{B}] = i\hat{C}; \quad (6)$$

thus, the uncertainty principle of these two operators is given by

$$\langle(\Delta\hat{A})^2\rangle\langle(\Delta\hat{B})^2\rangle \geqslant \frac{\langle\hat{C}\rangle^2}{4}. \quad (7)$$

Here, $\Delta\hat{A} = \hat{A} - \langle\hat{A}\rangle$ [21] and the irreducible lower bound in Eq. (1) is given by $\langle\hat{C}\rangle^2/4$.

In spherical coordinates, the generalized momentum operators, according to Dirac's definition [54], are

$$\hat{p}_r = -i\frac{\partial}{\partial r}, \quad \hat{p}_\theta = -i\frac{\partial}{\partial\theta}, \quad \hat{p}_\phi = -i\frac{\partial}{\partial\phi}, \quad (8)$$

which according to Eq. (6) obey the following commutation relations:

$$[\hat{r}, \hat{p}_r] = i, \quad [\hat{\theta}, \hat{p}_\theta] = i, \quad [\hat{\phi}, \hat{p}_\phi] = i. \quad (9)$$

From Eq. (7), their Heisenberg's inequalities are

$$\Delta\hat{r}\Delta\hat{p}_r \geqslant \tfrac{1}{2}, \quad \Delta\hat{\theta}\Delta\hat{p}_\theta \geqslant \tfrac{1}{2}, \quad \Delta\hat{\phi}\Delta\hat{p}_\phi \geqslant \tfrac{1}{2}. \quad (10)$$

However, $\hat{p}_r$ and $\hat{p}_\theta$ are not self-adjoint operators and thus their expectation values are completely imaginary, which implies that the obtained results are physically unacceptable [17], as stated by Deutsch in Ref. [55]: "*...except in the case of canonical conjugate observable, the generalized Heisenberg's inequality does not properly express the quantum uncertainty principle...*" Hence, the following expression for the correct quantum-mechanical canonical conjugate momentum operator to the variable r should be used [56–60]:

$$\hat{p}_r = \dot{\hat{r}} = -i[\hat{r}, \hat{H}] = -i\left[\frac{\partial}{\partial r} + \frac{1}{r}\right] = -i\frac{1}{r}\frac{\partial}{\partial r}r, \quad (11)$$

whose expectation value is null as shown by Hey [58], i.e., $\langle\hat{p}_r\rangle = 0$ for stationary states. This fulfills the modified Ehrenfest theorem [60,61] for spherical coordinates. From this, the radial variances for $\Delta\hat{r}$ and $\Delta\hat{p}_r$ are

$$\Delta\hat{r} = \sqrt{\langle\hat{r}^2\rangle - \langle\hat{r}\rangle^2} \quad \text{and} \quad \Delta\hat{p}_r = \sqrt{\langle\hat{p}_r^2\rangle}. \quad (12)$$

In order to study the effects produced by the confining cavity on the uncertainty principle within our FD implementation, the expectation value of the radial component of the square of the linear momentum is calculated from Eq. (5) as

$$\begin{aligned}\left\langle \hat{p}_r^2 \right\rangle &= 2\langle \hat{K} \rangle - \ell(\ell+1)\langle \hat{r}^{-2} \rangle \\ &= 2E + 2Z\langle \hat{r}^{-1} \rangle - \ell(\ell+1)\langle \hat{r}^{-2} \rangle. \end{aligned} \tag{13}$$

This is the expression we use to determine the variances and the uncertainty inequalities, whose results are discussed in Sec. III A.

C. Vector uncertainty principle

In the previous section, Sec. II B, the radial representation of Heisenberg's uncertainty relation is shown, which only considers the scalar expectation values. Now we focus on the vector representation of the position and momentum operators whereby the uncertainty relation is calculated [25,26,29,56]. That is, the expectation values are calculated on the position and the momentum vector operators.

In spherical coordinates the vector position is $\mathbf{r} = r\mathbf{e}_r$ while the momentum operator is given by

$$\hat{\mathbf{p}} = -i\nabla = -i\left\{ \mathbf{e}_r \frac{\partial}{\partial r} + \mathbf{e}_\theta \frac{1}{r}\frac{\partial}{\partial \theta} + \mathbf{e}_\phi \frac{1}{r\sin\theta}\frac{\partial}{\partial \phi} \right\}. \tag{14}$$

Here, $\mathbf{e}_r$, $\mathbf{e}_\theta$, and $\mathbf{e}_\phi$ are the spherical unit vectors. Therefore, according to Eq. (6) the commutator $[\hat{\mathbf{r}}, \hat{\mathbf{p}}] = -3i$, such that the uncertainty inequality, Eq. (1), for the vector case becomes

$$\Delta\hat{\mathbf{r}}\Delta\hat{\mathbf{p}} \geqslant \tfrac{3}{2}. \tag{15}$$

However, Eq. (15) has a generalization for spherically symmetric potentials [26,56,62] involving the angular momentum quantum number ℓ, as

$$\Delta\hat{\mathbf{r}}\Delta\hat{\mathbf{p}} \geqslant \ell + \tfrac{3}{2}, \tag{16}$$

with

$$\Delta\hat{\mathbf{r}} = \sqrt{\langle \hat{\mathbf{r}}^2 \rangle - \langle \hat{\mathbf{r}} \rangle^2}, \quad \Delta\hat{\mathbf{p}} = \sqrt{\langle \hat{\mathbf{p}}^2 \rangle - \langle \hat{\mathbf{p}} \rangle^2}. \tag{17}$$

Due to the radial symmetry, we have that $\langle \hat{\mathbf{r}} \rangle = \mathbf{0}$. Furthermore, the expectation value for $\hat{\mathbf{r}}^2$ is $\langle r^2 \rangle$, since $\hat{\mathbf{r}}^2 = \hat{\mathbf{r}} \cdot \hat{\mathbf{r}} = \hat{r}^2$, and $\langle \hat{\mathbf{p}} \rangle = \mathbf{0}$ for stationary states, such that Eqs. (17) simplify to

$$\Delta\hat{\mathbf{r}} = \sqrt{\langle \hat{r}^2 \rangle} \quad \text{and} \quad \Delta\hat{\mathbf{p}} = \sqrt{\langle \hat{p}^2 \rangle}. \tag{18}$$

Again, $\langle \hat{p}^2 \rangle$ is related to the kinetic energy through Eq. (2),

$$\langle \hat{p}^2 \rangle = 2\langle \hat{K} \rangle = 2\langle E - \hat{V} \rangle = 2E + 2Z\langle \hat{r}^{-1} \rangle. \tag{19}$$

The expectation value of the radial momentum $\langle \hat{p}_r^2 \rangle$ is related to the angular momentum square as

$$\langle \hat{p}^2 \rangle = \left\langle \hat{p}_r^2 \right\rangle + \ell(\ell+1)\langle \hat{r}^{-2} \rangle. \tag{20}$$

Thus, the radial case involves the state structure of the atom, while the vector case does not, as seen from Eqs. (13) and (19), since in the radial case we have the centrifugal potential.

D. Numerical implementation

In order to evaluate Eqs. (12) and (18), we solve the Schrödinger equation, Eq. (5), and calculate the variances in a numerical mesh through an FD approach as reported in Ref. [63]. For this case, we use an exponential grid, where

$$r_i = \exp\left[\frac{i\ln(r_o+1)}{N+1}\right] - 1, \tag{21}$$

and $i = 0, 1, 2, \ldots, N+1$, which takes care of the cusp behavior of the wave function for $r \to 0$. We use $N = 2000$ in the interval $0 < r < r_o$ for cavity sizes from $r_o = 1$ up to $r_o = 200$. We solve the linear algebra problem using MATHEMATICA [64].

At this stage, we point out that, in all cases, the accuracy of the eigenfunctions and energy calculations through the FD approach for the confined system shows excellent quantitative agreement with the exact ones with a precision on the fifth decimal place.

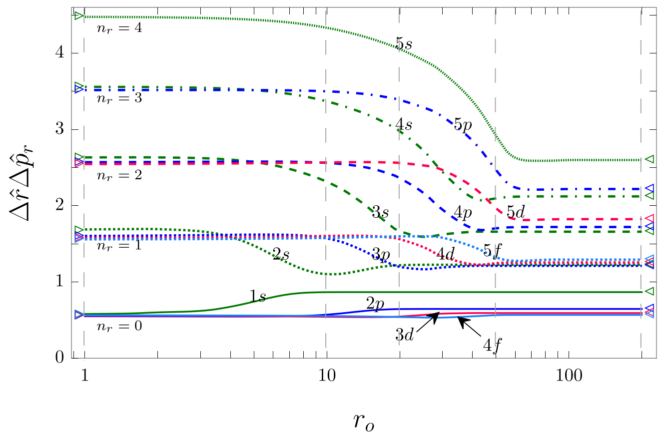

FIG. 1. Heisenberg's uncertainty principle values for the radial representation $\Delta\hat{r}\Delta\hat{p}_r$ as a function of the cavity radius r_o, for $n\ell$ states with $n = 1, 2, 3, 4, 5$ and $\ell = 0, 1, 2, 3$ of a confined H atom by an impenetrable spherical cavity. Here, n_r indicates the number of nodes for each state. ns states in green, np states in blue, nd states in red, and nf states in light blue. The vertical dashed lines indicate values of the uncertainty relation for cavity radii $r_o = 1$, 10, 20, 50, and 200 for the different states (see Table I). Symbols ($\triangleright$) at $r_o = 1$ and ($\triangleleft$) at $r_o = 200$ correspond to a particle-in-a-box and a free H atom, respectively.

III. RESULTS AND DISCUSSION

In this section, we analyze confinement effects on Heisenberg's uncertainty principle for a hydrogen atom ($Z = 1$) enclosed by a hard spherical cavity of radius r_o. Both the radial and vector representation are used to establish differences in their description on Heisenberg's uncertainty behavior. We complement our results of the confined H atom [56,58] with those of a particle-in-a-box [65] ($Z = 0$).

A. Radial uncertainty principle

The behavior of the radial uncertainty relations for the lowest $n \leqslant 5$ ($\ell = 0, 1, 2, 3$) states of the spherically confined H atom as a function of the cavity radius r_o is shown in Fig. 1. Firstly, we find that the states of this system that have the lowest values of their Heisenberg's uncertainty relation for the radial component, $\Delta\hat{r}\Delta\hat{p}_r \geqslant 1/2$, are those whose wave functions do not have any nodes, in agreement with Hey [58] for the free atom, as expected. On the other hand,

TABLE I. Radial Heisenberg's uncertainty values $\Delta\hat{r}\Delta\hat{p}_r$ for a particle-in-a-box, a confined (for a selected set of radii r_o), and a free H atom, according to the number of nodes.

		$\Delta\hat{r}\Delta\hat{p}_r^{(\mathrm{part})}$-particle	$\Delta\hat{r}\Delta\hat{p}_r$-confined H atom					$\Delta\hat{r}\Delta\hat{p}_r^{(\mathrm{free})}$-Hey [58]
n_r	State	$1 \leqslant r_o \leqslant 200$	$r_o = 1$	$r_o = 10$	$r_o = 20$	$r_o = 50$	$r_o = 200$	$r_o = \infty$
0	$1s$	0.5679	0.5799	0.8652	0.8660	0.8660	0.8660	0.8660
	$2p$	0.5514	0.5497	0.5708	0.6438	0.6455	0.6455	0.6455
	$3d$	0.5574	0.5561	0.5421	0.5458	0.5916	0.5916	0.5916
	$4f$	0.5632	0.5624	0.5529	0.5392	0.5638	0.5669	0.5669
	$5g$	0.5679	0.5674	0.5613	0.5522	0.5297	0.5528	0.5528
	$6h$	0.5718	0.5714	0.5673	0.5614	0.5338	0.5436	0.5436
1	$2s$	1.6703	1.6880	1.1023	1.2192	1.2248	1.2248	1.2247
	$3p$	1.5973	1.6028	1.5707	1.1979	1.2108	1.2108	1.2108
	$4d$	1.5725	1.5755	1.6029	1.5593	1.2453	1.2550	1.2550
	$5f$	1.5562	1.5581	1.5775	1.5977	1.3237	1.2918	1.2918
2	$3s$	2.6272	2.6328	2.3124	1.6658	1.6583	1.6583	1.6583
	$4p$	2.5665	2.5699	2.5609	2.3607	1.7026	1.7200	1.7200
	$5d$	2.5428	2.5455	2.5670	2.5600	1.9666	1.8229	1.8229
3	$4s$	3.5580	3.5578	3.3673	2.9755	2.0955	2.1213	2.1213
	$5p$	3.5141	3.5153	3.4993	3.3860	2.4669	2.2183	2.2183
4	$5s$	4.4790	4.4757	4.3321	4.0545	2.9170	2.5981	2.5981

for large cavity radii ($r_o > 100$) the uncertainty values tend toward those of the free hydrogen atom, whereas for small radii ($r_o < 2$), they converge to the values of a particle-in-a-box under the same confinement conditions. The values of the variances for momentum and position of a free H atom and a particle-in-a-box have been calculated from the exact solutions of the corresponding Schrödinger equation. In the case of the free atom the following expression, reported by Hey [58], is used to calculate the values reported in Table I:

$$\Delta\hat{r}\Delta\hat{p}_r^{(\mathrm{free})} = \frac{1}{2n}\sqrt{\frac{[n^2(n^2+2)-\ell^2(\ell+1)^2][n(2\ell+1)-2\ell(\ell+1)]}{n(2\ell+1)}}. \tag{22}$$

Also, Fig. 1 shows the behavior for the radial uncertainty relation as the cavity radius is reduced, indicating its dependence on the degree of competition between the Coulombic potential and the effect of the wall for a given cavity radius. Moreover, one notices a pattern in both limits, $r_o \to 0$ and $r_o \to \infty$, where states with the same number of nodes are grouped in bunches, as observed in Table I and indicated by vertical dashed lines at $r_o = 1$ and 200 in Fig. 1. This leads to the existence of well-defined gaps at these two limits. For a particle-in-a-box, the exact expressions are cumbersome since they rely on the zeros of the spherical Bessel functions. However, once they have been calculated, we find that Heisenberg's uncertainty relations are constant for each state and independent of the values of r_o, i.e.,

$$\Delta\hat{r}\Delta\hat{p}_r^{(\mathrm{part})} = \text{constant}. \tag{23}$$

For a hydrogen atom and for $r_o > 60$, one observes a bunching around the following values,: $\Delta\hat{r}\Delta\hat{p}_r \approx 0.5$ for nodeless states, $\Delta\hat{r}\Delta\hat{p}_r \approx 1$ for states with a single node, increasing by ≈0.5 as the number of nodes n_r increases. From Fig. 1, we infer that

$$\lim_{r_o \gg 1} \Delta\hat{r}\Delta\hat{p}_r \approx \frac{n_r+1}{2} = \frac{n-\ell}{2}, \tag{24}$$

which is a simplified version of Eq. (22), since at the limit $n \to \infty$, $\Delta\hat{r}\Delta\hat{p}_r^{(\mathrm{free})} \approx n/2$. On the other hand, for $r_o \to 0$, one notices that the uncertainty relations are grouped around $\Delta\hat{r}\Delta\hat{p}_r \sim 0.5$ for nodeless states, $\Delta\hat{r}\Delta\hat{p}_r \sim 1.5$ for single node states, an so on. Therefore, we infer

$$\lim_{r_o \to 0} \Delta\hat{r}\Delta\hat{p}_r \approx n_r + \tfrac{1}{2} = n - \ell - \tfrac{1}{2} \tag{25}$$

for a confined H atom. From Fig. 1, one sees that the differences in the $\Delta\hat{r}\Delta\hat{p}_r$ values between two states with consecutive number of nodes is around ∼1. But this just occurs for states with a small value of n, since as n increases, these differences decrease.

Some representative values for the radial component of the uncertainties for a particle-in-a-box, a confined H atom (inside a small cavity with $r_o = 1$, a larger cavity with $r_o = 200$, and some intermediate values of r_o), and a free H atom are listed in Table I for completeness.

Figure 2 shows the uncertainty values as a function of the principal quantum number n, for three values of the confining radius. For strong confinement regime, $r_o = 1$ (blue); for intermediate regime, $r_o = 40$ (red); and for weak confinement regime, $r_o = 100$ (green), as well as the values of the free atom [58] (⋆ symbols). One notes that, for the free case, the uncertainty values show a trend of increasing as n increases, except for $n_r = 0$. But, for small confining radii this trend is reversed, and gives as a result that the lowest excited states (small n) are "fuzzier" than the highest ones. On the other hand, the confinement induces an increment of the uncertainty values for almost all states, except for some nodeless states, $1s$, $2p$, $3d$, and $4f$ ($n_r = 0$). These lowest states become "sharper" as

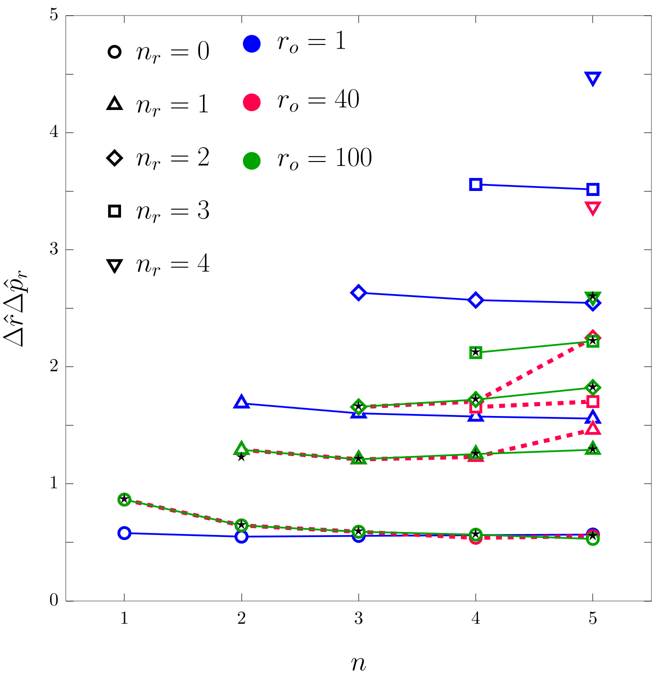

FIG. 2. Uncertainty principle values as a function of the principal quantum number n. Values of the radial quantum number $n_r = n - \ell - 1$ are indicated by a common symbol. The lines joining the points are used to guide the eye. The same color lines and symbols correspond to the same confining radius; blue to $r_o = 1$, red to $r_o = 40$, and green to $r_o = 100$. ($\star$) symbols correspond to the values of the free atom, as reported by Hey [58].

the system reaches the strong confinement regime. Within the transition region—for instance, $r_o = 40$—one recognizes that the uncertainty values show a larger increment as n increases, for a state with the same number of nodes n_r.

Now, let us recall that in quantum mechanics, the states that satisfy the minimum value of Heisenberg's uncertainty relation are the ground state of the harmonic oscillator and the Gaussian wave packet for a free particle [21,22,25,56]. These states are so-called coherent states. From Eq. (22) or (24) one verifies that, for nodeless Rydberg states ($n \gg 1$ and $\ell = n - 1$) of the free atom, the product $\Delta\hat{r}\Delta\hat{p}_r^{(\mathrm{free})}$ tends to the minimum value of Heisenberg's uncertainty principle, i.e.,

$$\lim_{n\to\infty} \Delta\hat{r}\Delta\hat{p}_r^{(\mathrm{free})} = \lim_{n\to\infty} \frac{1}{2}\sqrt{\frac{2n+1}{2n-1}} = \frac{1}{2}. \tag{26}$$

Thus, as the principal quantum number n increases, the nodeless states tend to become pseudo-classical states, in agreement with Bohr's correspondence principle [22,66]. Consequently, for nodeless states with $n \to \infty$

$$\lim_{n\to\infty} \psi_{n,n-1}^{(\mathrm{free})} = \text{pseudo-classical state} \tag{27}$$

and the inequality $\Delta\hat{r}\Delta\hat{p}_r^{(\mathrm{free})}$ is bounded by the lowest value 0.5 and the value for the ground state of the free atom, 0.866 03. For instance, if we consider the free atom state with $n = 100$ and $\ell = 99$, we have that $\Delta\hat{r}\Delta\hat{p}_r^{(\mathrm{free})} = 0.50251$. The coherence of this state is observed in Fig. 3, where the wave function (solid blue line) is compared to a Gaussian function (black dashed line), showing the similarities between them,

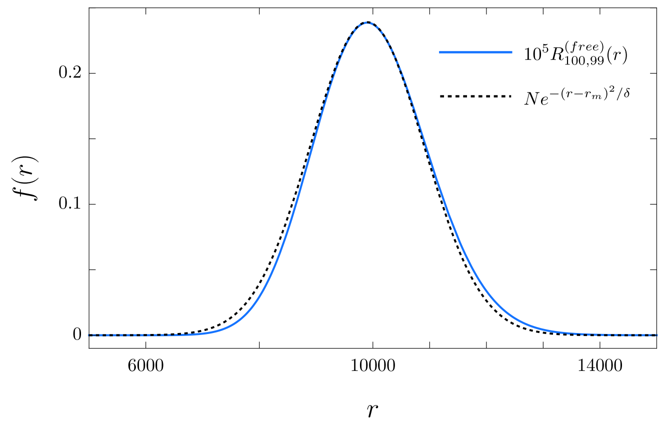

FIG. 3. Radial wave function of a free H atom $R_{n,\ell}^{(\mathrm{free})}(r)$ (solid blue line) for $n = 100$ and $\ell = 99$ and Gaussian wave function, $Ne^{-(r-r_m)^2/\delta}$ (dashed black line), with adjusted parameters $N = 0.239$, $r_m = 9900$, and $\delta = 5\times 10^7$.

thus confirming our results. On the contrary, for the case of the same nodeless state for a particle-in-a-box ($n = 100$ and $\ell = 99$), it has an uncertainty value of $\Delta\hat{r}\Delta\hat{p}_r^{(\mathrm{part})} = 0.6069$, which is higher than the corresponding value of the ground state, $\Delta\hat{r}\Delta\hat{p}_r^{(\mathrm{part})} = 0.5679$ (see Table I). Owing to the fact that for strong confinement conditions the kinetic energy overrides the Coulombic potential energy, the electron of the H atom behaves more like a particle-in-a-box [65]; this is the reason we compare the values for both systems within the strong confinement regime, finding that they are very similar.

From the previous discussion, the arrangement of the radial uncertainty of the nodeless states of a confined H atom is different under strong confinement conditions when compared to the uncompressed system. In this case, the following arrangement $2p < 3d < 4f < 1s < 5g < 6h < \cdots$ is observed (see Table I). Therefore, we expect that the $2p^{(\mathrm{part})}$ wave function of a particle-in-a-box to be similar to a Gaussian function. This is observed in Fig. 4, where the solid blue line corresponds to the spherical Bessel function of the $2p^{(\mathrm{part})}$

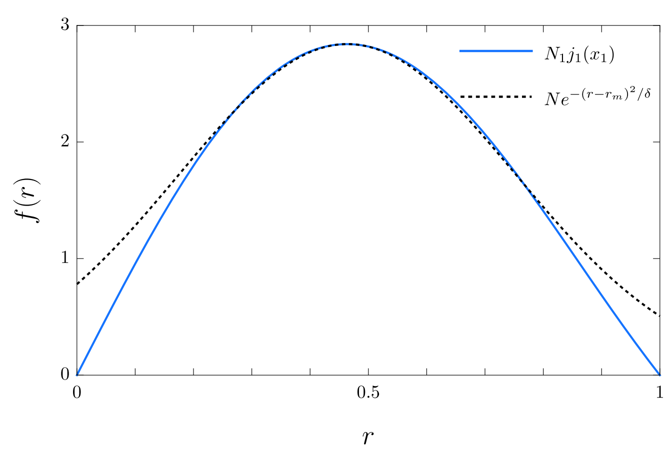

FIG. 4. Radial wave function of a particle-in-a-box $N_1 j_1(x_1)$ (solid blue line), corresponding to the $2p^{(\mathrm{part})}$ state and Gaussian wave function, $Ne^{-(r-r_m)^2/\delta}$ (dashed black line), with adjusted parameters $N = 2.84$, $r_m = 0.464$, and $\delta = 1/6$.

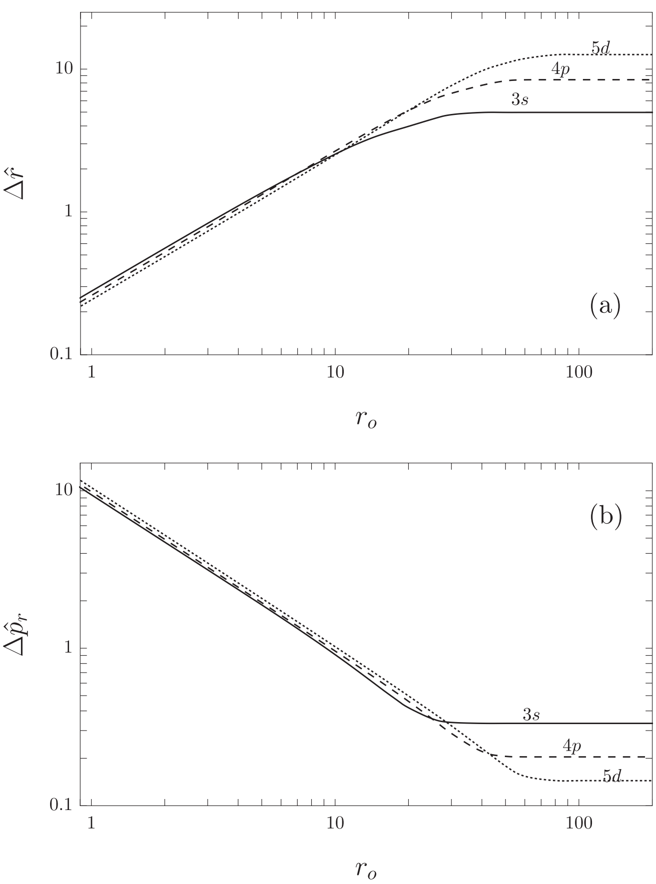

FIG. 5. $\Delta\hat{r}$ and $\Delta\hat{p}_r$ uncertainties as a function of the confinement radius r_o for an impenetrable spherical cavity, for $3s$, $4p$, and $5d$ states of a confined H atom.

state and the dashed black line to the Gaussian function. First, one notes a really good agreement in the vicinity of the center of the Gaussian at $r_m = 0.464$, but as we move away from r_m the boundary modifies the function, since it suddenly vanishes at $r = 0$ and $r = r_o$. Thus, it is the confinement (boundary conditions) that prevents the uncertainty principle from reaching its minimum value. However, the same confinement conditions are responsible for making some nodeless states to evolve from low to high coherence, for the hydrogen case. For instance, consider the nodeless $1s$, $2p$, $3d$, and $4f$ states of the confined H atom, whose uncertainty values decrease as the confinement radius r_o decreases. On the contrary, for higher excited nodeless states, the product $\Delta\hat{r}\Delta\hat{p}_r$ increases as the cavity size decreases, which means these states become less coherent as the cavity size is reduced. So the confinement makes a nodeless Rydberg states of the confined atom less coherent.

The behavior of $\Delta\hat{r}$ and $\Delta\hat{p}_r$ for the $3s$, $4p$, and $5d$ states with two nodes is shown in Fig. 5. One notes that for large confinement radii the variances $\Delta\hat{r}$ and $\Delta\hat{p}_r$ have constant values, which correspond to the values of the free H atom, whereas for small radii their values tend to the corresponding values of a particle-in-a-box, whose dependencies are $\Delta\hat{r}^{(\text{part})} \propto r_o$ and $\Delta\hat{p}_r^{(\text{part})} \propto r_o^{-1}$. Firstly, the behavior of the variance $\Delta\hat{r}$ [Fig. 5(a)] can be understood from Eq. (12) under the assumption that for strong confinement $\langle\hat{r}^2\rangle \propto \langle\hat{r}\rangle^2$ such that $\Delta\hat{r} \propto \langle\hat{r}\rangle \approx 0.3r_o$, i.e., it is proportional to the cavity size. With the same reasoning, we find that, from Fig. 5(b), $\Delta\hat{p}_r \approx 10/r_o$. Therefore, we use this matching to explain what is happening on the product $\Delta\hat{r}\Delta\hat{p}_r$ of the confined H atom. For both systems and small confinement radii, the position expectation value $\langle\hat{r}\rangle$ tends to converge to the value $r_o/2$. For example, the position expectation value $\langle\hat{r}\rangle$ for the $ns^{(\text{part})}$ state of a particle-in-a-box is exactly $r_o/2$ for all r_o, as expected. Moreover, for the $ns^{(\text{part})}$ states, the arrangement of the expectation values of the square of the position $\langle\hat{r}^2\rangle$ is $1s^{(\text{part})} < 2s^{(\text{part})} < 3s^{(\text{part})} < 4s^{(\text{part})} < 5s^{(\text{part})}$. From these results one concludes that the variances $\Delta\hat{r}^{(\text{part})}$ keep the same order as $\langle\hat{r}^2\rangle$ since $\langle\hat{r}\rangle = r_o/2$ for all $ns^{(\text{part})}$ states of a particle-in-a-box. On the other hand, the position expectation value of the ns states in the confined H atom only reaches the value $r_o/2$ at $r_o = 0.1$, which is smaller than the smallest radius reported here. Thus, for small cavity sizes, the $\Delta\hat{r}\Delta\hat{p}_r$ values show the same order as the corresponding ones of a particle-in-a-box. Other particle-in-a-box states with $\ell \neq 0$ do not show the same behavior, since the centrifugal potential $\ell(\ell+1)/r^2$, as observed in Eq. (13), plays an important role in the position expectation value, hence it is slightly larger than $r_o/2$ as ℓ increases. This can be compared to the confined H atom within the strong confinement regime such that, for the same confinement radius, the more extended wave functions are squeezed by the effect of the wall. For a cavity size $r_o = 1$, the expectation values, $\langle\hat{r}\rangle$ and $\langle\hat{r}^2\rangle$, of both systems (confined H atom and particle-in-a-box) have similar values, and therefore they show the following order: for the np states, $2p > 3p > 4p > 5p$; for the nd states, $3d > 4d > 5d$; and for the nf states, $4f > 5f$, such that the value of the variance $\Delta\hat{r}$ (in both systems) is lower for more extended wave functions related to higher excited states. For instance, consider the $nd^{(\text{part})}$ states of a particle-in-a-box, where we have $\Delta\hat{r}_{3d}^{(\text{part})} < \Delta\hat{r}_{4d}^{(\text{part})} < \Delta\hat{r}_{5d}^{(\text{part})}$ (dashed black lines), as shown in Fig. 6(a). In summary, for large confinement radii, the states with the most extended wave functions have a larger value of $\Delta\hat{r}$, but as the confinement conditions become more extreme these extended wave functions are squeezed stronger, which results in a lower value of $\Delta\hat{r}$ than for less extended wave functions. For example, for small confinement radii one can observe that, for the confined H atom, the $3s$ state has a higher $\Delta\hat{r}$ value than the $4p$ and $5d$ states [see Fig. 5(a)].

The behavior of the variance $\Delta\hat{p}_r$ as a function of the confining cavity size is depicted in Fig. 5(b) for the $3s$, $4p$, and $5d$ states, while Fig. 6(b) shows the same for the nd states (with $n = 3$, 4, and 5) of the confined H atom (solid blue lines) and the corresponding uncertainty values of a particle-in-a-box (dashed black lines). At first, for large values of r_o the radial kinetic energy is lower for states with a more extended wave function. This indicates that the electron moves faster toward the nucleus than away from it. But, as the cavity size decreases, the electron gains more and more radial kinetic energy. This is due to the effect of the wall when compared to the Coulombic potential, which squeezes the wave function and leads to a decrease of $\Delta\hat{r}$. In order to satisfy Heisenberg's uncertainty principle, $\Delta\hat{p}_r$ must increase. From Figs. 5(b) and 6(b), we find that, for smaller r_o, the value of $\Delta\hat{p}_r$ of the enclosed H atom converges to the values of a particle-in-a-box.

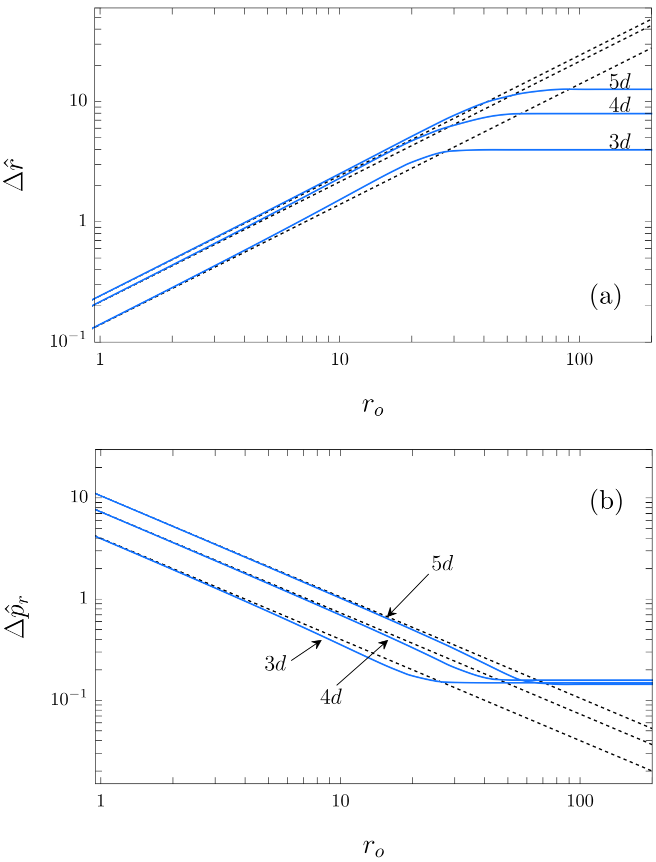

FIG. 6. $\Delta\hat{r}$ and $\Delta\hat{p}_r$ uncertainties as a function of the confinement radius r_o for nd states with $n = 3, 4, 5$ of a confined H atom (solid blue lines) and a particle-in-a-box (dashed black lines) as a function of an impenetrable spherical cavity radius r_o.

For states with the same number of nodes, the values of the variances $\Delta\hat{r}$ are very similar, as observed in Fig. 5(a), and similarly for the variances in $\Delta\hat{p}_r$, as shown in Fig. 5(b). Consequently, the product $\Delta\hat{r}\Delta\hat{p}_r$ has very similar values and exhibits the arrangement in bunches as shown in Fig. 1. We notice that there are minima in the transition range, from large to small cavity sizes. For instance, consider the $4d$ state, whose value of $\Delta\hat{r}\Delta\hat{p}_r$ as a function of r_o is plotted in Fig. 1 (dashed red line). For large radii, it keeps a constant value until reaching $r_o \sim 50$. At this point, its value decreases until reaching a minimum value at around $r_o \sim 41$, and later starts increasing around $r_o \sim 40$. Finally, it reaches a constant value, for $r_o < 20$, which corresponds to the value of a particle-in-a-box. Notice in Fig. 6(a) that $\Delta\hat{r}$ decreases faster between $r_o = 50$ and $r_o = 40$, while in this same interval $\Delta\hat{p}_r$ [Fig. 6(b)] remains almost constant. In a recent work, Estañon *et al.* [31] observed the same behavior for the confined H atom but in two dimensions. This behavior is due to the competition between the kinetic and Coulombic potential energy. First, the variances $\Delta\hat{r}^{(\text{part})}$ and $\Delta\hat{p}_r^{(\text{part})}$ of a particle-in-a-box are proportional to r_o and r_o^{-1}, respectively, such that Eq. (23) is satisfied. From Fig. 6 one recognizes that $\Delta\hat{r}$ and $\Delta\hat{p}_r$ dependence are $\Delta\hat{r} \propto r_o^{\alpha_{\Delta\hat{r}}}$ and $\Delta\hat{p}_r \propto r_o^{\alpha_{\Delta\hat{p}_r}}$, with $\alpha_{\Delta\hat{r}} \geqslant 0$ and $\alpha_{\Delta\hat{p}_r} \leqslant 0$. Here, we notice that for the $4d$ state, as r_o decreases, $\Delta\hat{p}_r$ increases slower than r_o^{-1}. This occurs for $20 < r_o < 40$, with $\Delta\hat{p}_r \sim r_o^{-1.1}$. But, in this same interval $\Delta\hat{r} \sim r_o^{0.63}$, thus the product $\Delta\hat{r}\Delta\hat{p}_r \sim r_o^{-0.47}$. This behavior leads to an increment of $\Delta\hat{r}\Delta\hat{p}_r$ as r_o decreases.

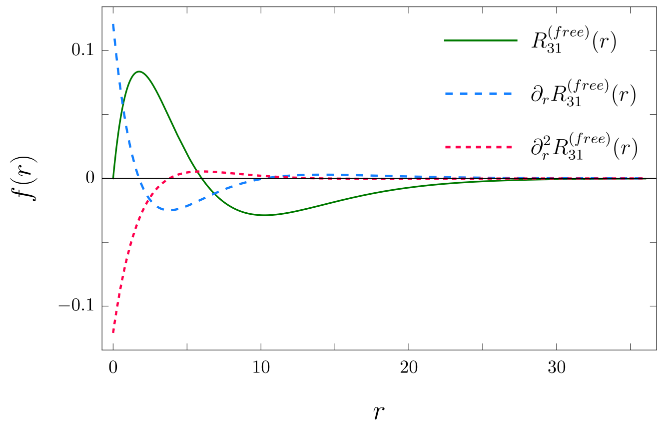

FIG. 7. Radial wave function (solid line) and its first (dashed line) and second derivative (dotted line) as a function of the radial coordinate for the $3p^{(\text{free})}$ state of a free H atom.

Finally, for $r_o < 10$, $\Delta\hat{r}$ and $\Delta\hat{p}_r$ tend to the corresponding values of the particle-in-a-box, r_o and r_o^{-1}, respectively, which gives a constant value observed for small r_o. These behaviors are more evident if we consider a higher excited state. Here, we have just discussed a few states to explain the radial uncertainty behavior. Since the variance $\Delta\hat{r}$ is related to the wave function and the variance $\Delta\hat{p}_r$ is related to its first and second derivative, the expectation value of the kinetic energy and the momentum are less sensitive to changes in the confining cavity size, as seen in Fig. 7. Here, one observes that the second derivative spans a less-extended function than that of the first derivative and the radial function. This means that the properties that depend on the first and second derivatives are less affected by the confinement than those depending on the radial function as the cavity size becomes smaller.

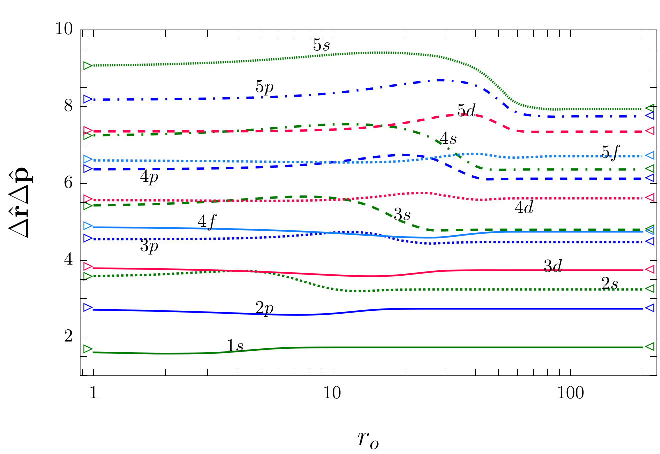

FIG. 8. Heisenberg's uncertainty values for the vector representation $\Delta\hat{\mathbf{r}}\Delta\hat{\mathbf{p}}$ as a function of the confinement radius r_o, for $n\ell$ states with $n = 1, 2, 3, 4, 5$ and $\ell = 0, 1, 2, 3$ for a confined H atom in an impenetrable spherical cavity. The line colors are the same as in Fig. 1. Symbols ($\triangleright$) at $r_o = 1$ and ($\triangleleft$) at $r_o = 200$ correspond to a particle-in-a-box and a free H atom, respectively.

TABLE II. Vector uncertainty values $\Delta\hat{\mathbf{r}}\Delta\hat{\mathbf{p}}$ for a confined H atom and a particle-in-a-box, under the same confinement conditions, for several radii r_o, as well as the exact value of the free H atom.

		$\mathcal{C}_{n\ell} = \Delta\hat{\mathbf{r}}\Delta\hat{\mathbf{p}}^{(\text{part})}$	$\Delta\hat{\mathbf{r}}\Delta\hat{\mathbf{p}}$-confined H atom					$\Delta\hat{\mathbf{r}}\Delta\hat{\mathbf{p}}^{(\text{free})}$-Hey [58]
n_r	State	$1 \leqslant r_o \leqslant 200$	$r_o = 1$	$r_o = 10$	$r_o = 20$	$r_o = 50$	$r_o = 200$	$r_o = \infty$
1	$1s$	1.6703	1.6026	1.7319	1.7320	1.7320	1.7320	1.7321
	$2p$	2.7502	2.7120	2.6111	2.7364	2.7386	2.7386	2.7386
	$3d$	3.8174	3.7927	3.6147	3.6241	3.7417	3.7417	3.7417
	$4f$	4.8762	4.8585	4.7110	4.6024	4.7369	4.7434	4.7434
	$5g$	5.9289	5.9155	5.7984	5.6847	5.6485	5.7446	5.7446
	$6h$	6.9769	6.9663	6.8719	6.7728	6.5945	6.7454	6.7454
2	$2s$	3.5580	3.5884	3.2577	3.2370	3.2404	3.2404	3.2404
	$3p$	4.5526	4.5495	4.7192	4.5050	4.4721	4.4721	4.4721
	$4d$	5.5743	5.5657	5.5723	5.7334	5.6008	5.6125	5.6125
	$5f$	6.6085	6.5991	6.5479	6.5856	6.6989	6.7082	6.7082
3	$3s$	5.3953	5.4287	5.6252	4.9927	4.7958	4.7958	4.7958
	$4p$	6.3613	6.3676	6.5512	6.7443	6.1127	6.1237	6.1237
	$5d$	7.3565	7.3551	7.4013	7.5721	7.5518	7.3484	7.3485
4	$4s$	7.2207	7.2522	7.5347	7.4205	6.3560	6.3639	6.3640
	$5p$	8.1723	8.1820	8.3502	8.5874	8.1733	7.7459	7.7460
5	$5s$	9.0414	9.0705	9.3523	9.3908	8.5041	7.9372	7.9373

In the following section, we discuss Heisenberg's uncertainty values for the vector case.

B. Vector uncertainty principle

Now, we present our results for Heisenberg's uncertainty principle in its vector representation, which complement our study of the H atom under spatial confinement conditions.

The uncertainty values $\Delta\hat{\mathbf{r}}\Delta\hat{\mathbf{p}}$ of the confined H atom as a function of the confinement radius r_o are shown in Fig. 8. From this figure one notes that they satisfy the generalized Heisenberg's uncertainty principle, Eq. (16), for all values of r_o. For instance, the ns states (green lines) have uncertainty values higher than $3/2$, where the lowest value corresponds to the $1s$ state (solid green line). For the np states (blue lines), they have values higher than $5/2$ and the lowest value is for the $2p$ state (solid blue line), and so on with higher ℓ. Notice that the nodeless states are the ones with the lowest value, according to Eq. (16). In this case, the uncertainty values do not present the bunching that is observed in the radial case (Fig. 1). This behavior is mainly due to the centrifugal potential, since it depends on the angular momentum quantum number ℓ, and its expectation value is added to $\langle \hat{p}_r^2\rangle$ to obtain $\langle \hat{p}^2\rangle$, Eq. (20).

For the free atom, the exact value for the product $\Delta\hat{\mathbf{r}}\Delta\hat{\mathbf{p}}^{(\text{free})}$ is [56,58]

$$\Delta\hat{\mathbf{r}}\Delta\hat{\mathbf{p}}^{(\text{free})} = \sqrt{\frac{5n^2+1-3\ell(\ell+1)}{2}}, \tag{28}$$

whereas, for a particle-in-a-box, we have that the product of its variances is also constant, as for the case of the radial representation,

$$\Delta\hat{\mathbf{r}}\Delta\hat{\mathbf{p}}^{(\text{part})}_{n\ell} = \mathcal{C}_{n\ell}(x_\nu) = \text{constant}. \tag{29}$$

Here, x_ν are the zeros of the spherical Bessel functions $j_\ell(x)$ (see Ref. [67]) and $\mathcal{C}_{n\ell}$ has a different value for each state.

Table II shows the vector uncertainty values $\Delta\hat{\mathbf{r}}\Delta\hat{\mathbf{p}}$ for a confined H atom and a particle-in-a-box, under the same confinement conditions, for several radii values r_o, as well as the exact value of the free H atom.

As in the radial case, the results for a particle-in-a-box help us to understand what is occurring with the confined atom under strong confinement conditions. Firstly, the variance of the position is a function of r_o and x_ν, i.e., $\Delta\hat{\mathbf{r}}^{(\text{part})}_{n\ell} = \Delta\hat{\mathbf{r}}^{(\text{part})}_{n\ell}(r_o, x_\nu)$. Since the analytical expressions for these uncertainty values are cumbersome, we only discuss the cases of the ns and nd states. For these cases one obtains

$$\begin{aligned}
\Delta\hat{\mathbf{r}}^{(\text{part})}_{ns} &= r_o\sqrt{\frac{4x_\nu^3 + 3\sin(2x_\nu) - 6x_\nu[\cos(2x_\nu) - x_\nu\sin(2x_\nu)]}{6x_\nu^2[2x_\nu - \sin(2x_\nu)]}}\\
\Delta\hat{\mathbf{r}}^{(\text{part})}_{nd} &= r_o\sqrt{\frac{4\big[x_\nu^4 + 9x_\nu^2 - 27\big] - 6\big[7x_\nu^2 - 18\big]\cos(2x_\nu) - 3x_\nu\big[2x_\nu^2 - 37\big]\sin(2x_\nu)}{6\big\{2\big[x_\nu^4 - 3x_\nu^2 - 3\big] - 6\big[x_\nu^2 - 1\big]\cos(2x_\nu) + x_\nu\big[x_\nu^2 - 12\big]\sin(2x_\nu)\big\}}}.
\end{aligned} \tag{30}$$

In contrast, for a particle-in-a-box, $\Delta\hat{\mathbf{p}}^{(\text{part})} = \sqrt{\langle \hat{p}^2\rangle} = \sqrt{2E} = k$, since the potential energy is zero inside the box and k is related to the zeros of the spherical Bessel functions with $r_o k = x_\nu$, hence

$$k_\nu = \frac{x_\nu}{r_o} = \Delta\hat{\mathbf{p}}^{(\text{part})}_{n\ell}. \tag{31}$$

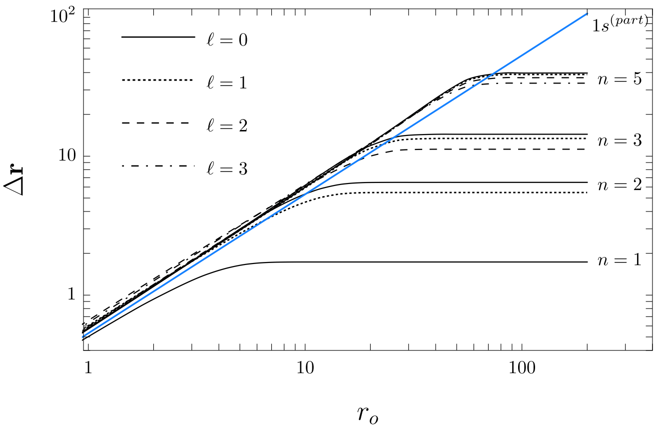

FIG. 9. Uncertainty $\Delta\hat{\mathbf{r}}$ as a function of the confinement radius r_o, for $n\ell$ states with $n = 1, 2, 3, 5$ and $\ell = 0, 1, 2, 3$ of a confined H atom (black lines) and $1s^{(\mathrm{part})}$ of a particle-in-a-box (solid blue line).

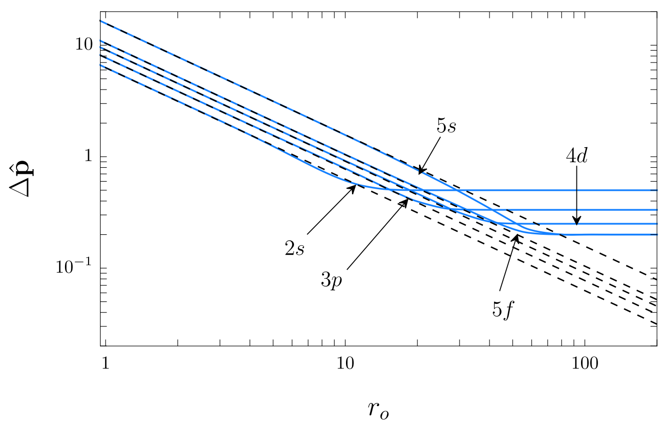

FIG. 10. Uncertainty $\Delta\hat{\mathbf{p}}$ as a function of the confinement radius r_o, for $2s$, $3p$, $4d$, and $5f$ states of a confined H atom (solid blue lines) and a particle-in-a-box (dashed black lines).

From Eqs. (30) and (31), the product $\Delta\hat{\mathbf{r}}\Delta\hat{\mathbf{p}}^{(\mathrm{part})}$ is calculated for each state as a function of r_o, obtaining the value of $\mathcal{C}_{n\ell}$ in Eq. (29). For instance, the $ns^{(\mathrm{part})}$ states for a particle-in-a-box have

$$\Delta\hat{\mathbf{r}}\Delta\hat{\mathbf{p}}^{(\mathrm{part})} = \sqrt{\frac{4x_\nu^3 + 3\sin(2x_\nu) - 6x_\nu[\cos(2x_\nu) - x_\nu\sin(2x_\nu)]}{6[2x_\nu - \sin(2x_\nu)]}}. \tag{32}$$

Here, the zeros x_ν of the spherical Bessel functions $j_o(x)$ are given by $x_\nu = n\pi$, $(n = 1, 2, 3, \ldots)$ as reported in Ref. [67]. Therefore, the uncertainty values for these states become

$$\Delta\hat{\mathbf{r}}\Delta\hat{\mathbf{p}}_{ns}^{(\mathrm{part})} = \sqrt{\frac{(n\pi)^2}{3} - \frac{1}{2}} = \mathcal{C}_{ns}. \tag{33}$$

If we consider higher $n\ell^{(\mathrm{part})}$ states, then x_ν are the zeros of the spherical Bessel function of order ℓ, $j_\ell(x)$.

After calculating the terms $\mathcal{C}_{n\ell}$ from Eq. (29), it is possible to obtain a simpler expression for $\Delta\hat{\mathbf{r}}^{(\mathrm{part})}$, which shows us its dependence with r_o

$$\Delta\hat{\mathbf{r}}_{n\ell}^{(\mathrm{part})} = \frac{\mathcal{C}_{n\ell}}{\Delta\hat{\mathbf{p}}^{(\mathrm{part})}} = \frac{\mathcal{C}_{n\ell}}{x_\nu} r_o, \tag{34}$$

which is linear as confirmed in Fig. 9 (solid blue line). Moreover, from Eq. (31) one obtains the energy for a particle-in-a-box as

$$E_{ns}^{(\mathrm{part})} = \frac{(\Delta\hat{\mathbf{p}})^2}{2} = \frac{x_\nu^2}{2}\frac{1}{r_o^2}. \tag{35}$$

Equations (31), (34), and (35) give us an idea of a simple dependence for Heisenberg's uncertainty and energy relations for a hydrogen atom confined by a spherical cavity of size r_o, for strong confinement.

Figure 9 shows the uncertainty $\Delta\hat{\mathbf{r}}$ as a function of the confinement radius r_o. Black lines represent the behavior of the $n\ell$ states, with $n = 1, 2, 3, 5$ and $\ell = 0, 1, 2, 3$, of the H atom, while the solid blue line corresponds to the $1s^{(\mathrm{part})}$ state of a particle-in-a-box. According to Eq. (34) it is a straight line, with $\Delta\hat{\mathbf{r}}^{(\mathrm{part})} = 1.6703 r_o/\pi$. We only plot the $1s^{(\mathrm{part})}$ state because the other ones have very similar behavior. In contrast to the radial case for $r_o \to 0$, here the grouping in bunches, according to the number of nodes, is not observed since all the states degenerate around the same value of $\Delta\hat{\mathbf{r}}$. This indicates that the observed splitting in the vector uncertainty values, in Fig. 8, comes from the centrifugal barrier, as mentioned before. Notice that the vector variance $\Delta\hat{\mathbf{r}}$ shows a very similar behavior to that of the radial component $\Delta\hat{r}$, since both have constant values for large radii, which are proportional to n^2, while for small radii they have a linear dependence on r_o. In contrast, from Fig. 9 and for large radii $r_o \to \infty$, one observes that the values of $\Delta\hat{\mathbf{r}}$ are grouping according to the value of n. Here, one sees the ground state with the lowest value, while the states with $n = 2$ have a higher value and higher excited states are grouping into well-defined bunches. This is expected from the exact value of $\Delta\hat{\mathbf{r}}^{(\mathrm{free})}$ of the free H atom [58,59]

$$\Delta\hat{\mathbf{r}}^{(\mathrm{free})} = \sqrt{\frac{n^2}{2}[5n^2 + 1 - 3\ell(\ell+1)]}, \tag{36}$$

where in the limit $n \to \infty$, it goes to $\Delta\hat{\mathbf{r}}^{(\mathrm{free})} \sim n^2\sqrt{5/2}$. Moreover, as ℓ increases, the $\Delta\hat{\mathbf{r}}^{(\mathrm{free})}$ value for that state is a bit lower than any state with the same value of n. That is similar to Bohr's classical model of the atom for a classical electron moving around the nucleus in a well-defined orbit determined by the principal quantum number n.

The $\Delta\hat{\mathbf{p}}$ uncertainty of a confined H atom (solid blue lines) and a particle-in-a-box (dashed black lines) as a function of r_o is shown in Fig. 10. Here, one observes the splitting between the values of $\Delta\hat{\mathbf{p}}$ for states with the same number of nodes, e.g., $2s$, $3p$, $4d$, and $5f$ states, in the region of small confinement radii, which does not occur for the radial case. This behavior is due to the centrifugal potential in Eq. (20). However, both cases share certain similarities, e.g., they have constant values for large r_o and the same dependence on the cavity radius since $\Delta\hat{\mathbf{p}} \propto r_o^{-1}$ for small cavity sizes. Also, the electron of the confined atom and the particle-in-a-box reach almost the same value of their respective momentum uncertainty, i.e., $\Delta\hat{\mathbf{p}} \approx \Delta\hat{\mathbf{p}}^{(\mathrm{part})}$, for confinement radii $r_o < 10$.

Now, the variance $\Delta\hat{\mathbf{p}}^{(\text{free})}$ for the free H atom is degenerate in n, since

$$\Delta\hat{\mathbf{p}}^{(\text{free})} = \frac{1}{n}. \tag{37}$$

From Fig. 10, one also observes the splitting of $\Delta\hat{\mathbf{p}}$ values for states with the same n as the cavity size is reduced—for instance, the $5s$ and $5f$ states. This splitting results in two phenomena. The first one is the splitting of the kinetic and total energy spectra of the hydrogen atom under confinement conditions [52,68], and the second one is the influence of the exerted strength by the wall as prescribed by the virial theorem for the confined system [69]. Thus, the electron not only moves on certain average distances (orbits) around the nucleus, as shown in Fig. 9, but it also moves with a well-defined momentum according to the energy level given by the principal quantum number n as allowed by the confinement. The value of the momentum decreases as the electron is in a higher excited state, in analogy to the classical system. As a result of the confinement effect, these averaged distances shrink and the degeneracy of the kinetic energy is broken, which gives rise to the breakdown of total energy degeneracy.

Unlike the radial case, in the vector case one observes that as r_o increases, the value of the product $\Delta\hat{\mathbf{r}}\Delta\hat{\mathbf{p}}$ increases from a constant value until reaching a global maximum; after this, it decreases and converges to the corresponding value of the free H atom, as seen in Figs. 1 and 8. This behavior is more evident for states with nodes and it results from the following factors. The sudden changes in the dependence on r_o for $\Delta\hat{\mathbf{r}}$ and $\Delta\hat{\mathbf{p}}$, since $\Delta\hat{\mathbf{r}} \propto r_o^{\alpha_{\Delta \mathbf{r}}}$ and $\Delta\hat{\mathbf{p}} \propto r_o^{\alpha_{\Delta \mathbf{r}}}$, where $\alpha_{\Delta\mathbf{r}}$ and $\alpha_{\Delta\mathbf{p}}$ are exponents, and they go from values of $\alpha_{\Delta\hat{\mathbf{r}}} \approx 1$ and $\alpha_{\Delta\hat{\mathbf{p}}} \approx -1$, for small cavity sizes, to their maximum values within the transition range, i.e., $\alpha_{\Delta\hat{\mathbf{r}}} > 1$ and $\alpha_{\Delta\hat{\mathbf{p}}} > -1$. Thereafter, for larger cavity sizes, the value of the exponents is such that $\alpha_{\Delta\hat{\mathbf{r}}} > 1$ and $\alpha_{\Delta\hat{\mathbf{p}}} < -1$, but $|\alpha_{\Delta\hat{\mathbf{r}}}| < |\alpha_{\Delta\hat{\mathbf{p}}}|$ where both $\Delta\hat{\mathbf{r}}$ and $\Delta\hat{\mathbf{p}}$ converge to constant values. This gives the behavior observed in Fig. 8, showing the global maxima. For instance, let us consider ns states. Since they have the same value of momentum in both radial and vector cases, because $\ell = 0$, see Eq. (20), then the difference between both behaviors, $\Delta\hat{r}\Delta\hat{p}_r$ and $\Delta\hat{\mathbf{r}}\Delta\hat{\mathbf{p}}$ (specifically the global maxima shown in Fig. 8), arises from the value of $\Delta\hat{\mathbf{r}}$. Our results show that $\alpha_{\Delta\hat{\mathbf{r}}}$, for the vector case, has a greater value on average than $\alpha_{\Delta\hat{r}}$, for the radial case. Both of them reach the value 1 for small radii.

In contrast to the radial case at the limit of large r_o, nodeless Rydberg states do not reach the minimum value of the generalized Heisenberg's uncertainty principle for the vector representation, Eq. (16), since their values are always larger than $\ell + 3/2$, as shown in Table II. For instance, the value of $\Delta\hat{\mathbf{r}}\Delta\hat{\mathbf{p}}$ for the ground state is $1.7321 > 3/2$, the minimum value for ns states, while the remaining nodeless states have even larger values, and the difference between the numerical results and the minimum in Eq. (16) increases as n increases. Therefore, the ground state is the most coherent state in the vector case and its coherence increases as the cavity size decreases, as observed in Fig. 8 and Table II.

Now, let us estimate the radii r_c at which the confinement begins to affect the electronic properties of the confined H atom. These radii r_c are estimated from the behavior of the momentum variances $\Delta\hat{\mathbf{p}}$, by finding the crossings, for two consecutive states with the same symmetry—in other words, the value of r_o where the electron in these two states has the same averaged momenta. Figure 11 shows the behavior of the variance $\Delta\hat{\mathbf{p}}$, as a function of r_o, for the ns and np states, respectively, as well as the crossing points between consecutive states with the same symmetry (dashed vertical lines). For instance, from Fig. 11(a) one observes that the $\Delta\hat{\mathbf{p}}$-crossing point between the $1s$ and $2s$ states is around $r_c \approx 6$, which is the radius r_c for the lowest state, $1s$, where the energy increment starts to rise with respect to the free atom, as the reader can verify in Ref. [52]. Likewise, the changes in the radial and vector uncertainty values for this state begin to be evident at this radius, as shown in Figs. 1 and 8. For higher excited ns states, the corresponding $\Delta\hat{\mathbf{p}}$-crossing points are $r_c \approx 17$, 33, and 52, which are related to the critical radii of the $2s$, $3s$, and $4s$ states, respectively. From Fig. 11(b) one observes another example of the $\Delta\hat{\mathbf{p}}$-crossing points, for the np states. The $\Delta\hat{\mathbf{p}}$-crossing point between the $4p$ and $5p$ states takes place at $r_c \approx 51$, which corresponds to the cavity radius for which the $4p$ state starts to feel the effect of the cavity, and so on with other states. A summary of these results is shown in Table III. Here, the values of $2\langle\hat{r}\rangle_{\text{free}}$ and the approximated numerical values of $\Delta\hat{\mathbf{p}}$-crossing points for some states are compared. Here, $\langle\hat{r}\rangle_{\text{free}}$ is the expectation value of the position of the free H atom. From the comparison of these two quantities, one realizes that $2\langle\hat{r}\rangle_{\text{free}}$ has a very

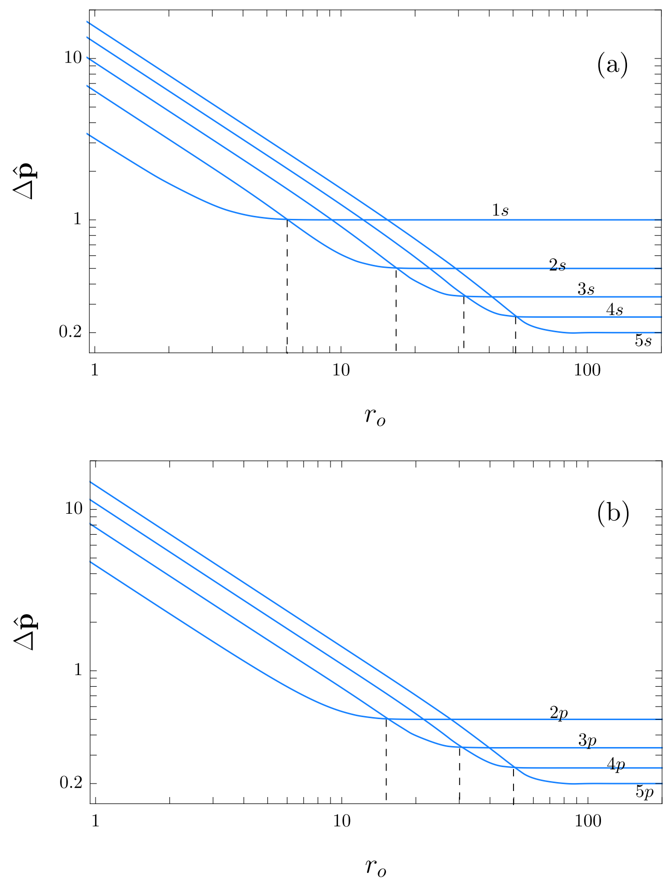

FIG. 11. $\Delta\hat{\mathbf{p}}$-crossing points as a function of the radius r_o for (a) the ns states ($n = 1, 2, 3, 4, 5$) and (b) the np states ($n = 2, 3, 4, 5$).

TABLE III. Critical cavity sizes r_c at which the state for a confined H atom exhibits considerable changes on its uncertainty principle due to the confinement.

State	$r_c = 2\langle \hat{r} \rangle_{\text{free}}$	$r_c = \Delta\mathbf{p}$-crossing
$1s$	3	6
$2s$	12	17
$3s$	27	33
$4s$	48	52
$2p$	10	16
$3p$	25	31
$4p$	46	51
$3d$	21	27
$4d$	42	49
$4f$	36	42

similar value to the $\Delta\hat{\mathbf{p}}$-crossing points, and this agreements is better as higher excited states are considered. Thus, we have two ways of estimating the critical radius r_c. From here, one concludes that the changes in the electronic properties of a confined atom mainly come from the increment in the kinetic energy ($\langle \hat{T} \rangle = \Delta\hat{\mathbf{p}}^2/2$) as the cavity size decreases. Thus, for $r_o < r_c$ one expects higher confinement effects. Moreover, the radius r_c gives an idea of the average size of the H atom orbital at which the cavity starts to affect it.

C. Relativistic limit

Now, what is the radius r_o for which relativistic effects start to be important? Since our analysis is not relativistic, the variances $\Delta\hat{\mathbf{p}}$, $\Delta\hat{p}_r$ and the energy diverge as r_o goes to zero, as shown in Eqs. (31) and (35). Thus, the electron mean square root velocity reaches and surpasses the speed of light c at some confinement radii, requiring relativistic corrections. Let us recall that the definition of the mean square root velocity is, from Eq. (12),

$$v_{\text{rms}} = \sqrt{\langle v^2 \rangle} = \sqrt{\langle \hat{p}^2 \rangle} = \Delta\hat{\mathbf{p}}, \tag{38}$$

for an electron with mass $m_e = 1$ (in atomic units). Let us consider that relativistic effects are important for particle velocities larger than 10% of the speed of light, i.e., $\Delta\hat{\mathbf{p}} > 0.1\,c$. Since $c \approx 137$ a.u., $\Delta\hat{\mathbf{p}} > 13.7$ for relativistic effects start to be important. To determine the cavity size at which this occurs, we start from those results of a particle-in-a-box, since for small radii the hydrogen atom under confinement has a similar behavior. In this case the energy is, from Eq. (35), $E = 13.7^2/2 = 93.845$. The corresponding radius that satisfies this condition is, from Eq. (31),

$$r_o \leqslant \frac{x_v}{13.7}. \tag{39}$$

Table IV shows the values of r_o and $\Delta\hat{\mathbf{r}}$ for each state from the $1s$ to $5f$ for which $\Delta\hat{\mathbf{p}}$ reaches the value $0.1\,c$. From here, one notes that the value of these two quantities (critical radius and $\Delta\hat{\mathbf{r}}$) increases for higher excited states, which is expected, since higher excited states have a higher energy value and as the system is being confined they reach the limit $\Delta\hat{\mathbf{p}} = 13.7$ (and $E = 93.845$) faster. We conclude that states, when $r_o < 1.1$, require a relativistic description of the confinement through the Dirac equation.

Another procedure to account for the relativistic correction is obtained from the time-independent perturbation theory [21]. Here, the perturbation term in the Hamiltonian comes from the kinetic energy, expressed in terms of the momentum and the speed of light, for relativistic motion

$$\hat{T} = c^2\left[\sqrt{1 + \frac{\hat{p}^2}{c^2}} - 1\right]; \tag{40}$$

expanding it in powers of the small $\hat{p}/c \ll 1$, we have

$$\hat{T} = \frac{\hat{p}^2}{2} - \frac{\hat{p}^4}{8c^2} + \frac{\hat{p}^6}{16c^4} + \cdots. \tag{41}$$

The first-order perturbation term is given by

$$\hat{H}' = -\frac{\hat{p}^4}{8c^2}, \tag{42}$$

such that the Hamiltonian is $\hat{H} = \hat{H}^{(0)} + \hat{H}'$, where $\hat{H}^{(0)}$ is the unperturbed Hamiltonian given by Eq. (2). The first-order correction to the energy is [21] thus

$$E^{(1)} = -\frac{1}{2c^2}[(E^{(0)})^2 + 2E^{(0)}\langle \hat{r}^{-1} \rangle + \langle \hat{r}^{-2} \rangle], \tag{43}$$

where $E^{(0)}$ is the energy of the unperturbed-confined system.

The nonrelativistic energy (solid blue lines) and the energy with relativistic correction (dashed black lines) of the confined H atom as a function of r_o are plotted in Fig. 12. First, for small radii, one confirms that the energy is proportional to r_o^{-2}, as in Eq. (35), corresponding to the energy of a particle-in-a-box. Here, one observes that the behavior of the energies exhibits a larger difference as the cavity size decreases. Moreover, the difference between both energies is greater as one considers higher excited states. In our case, the largest difference is for the $5s$ state, while the smallest one is for the ground state. To account for the relativistic

TABLE IV. Values of r_o and $\Delta\mathbf{r}$ for a-particle-in-a-box for which the electron velocity is 10% of the speed of light c, such that relativistic effects should be considered.

State	$r_o = \frac{x_v}{13.7}$	$\Delta\mathbf{r} = \frac{\mathcal{C}_{ns}}{13.7}$	State	$r_o = \frac{x_v}{13.7}$	$\Delta\mathbf{r} = \frac{\mathcal{C}_{np}}{13.7}$	State	$r_o = \frac{x_v}{13.7}$	$\Delta\mathbf{r} = \frac{\mathcal{C}_{nd}}{13.7}$	State	$r_o = \frac{x_v}{13.7}$	$\Delta\mathbf{r} = \frac{\mathcal{C}_{nf}}{13.7}$
$1s$	0.2293	0.1219									
$2s$	0.4586	0.2597	$2p$	0.3280	0.2007						
$3s$	0.6879	0.3938	$3p$	0.5639	0.3323	$3d$	0.4207	0.2786			
$4s$	0.9173	0.5271	$4p$	0.7959	0.4643	$4d$	0.6639	0.4069	$4f$	0.5101	0.3559
$5s$	1.1466	0.6599	$5p$	1.0267	0.5965	$5d$	0.8995	0.5370	$5f$	0.7604	0.4824

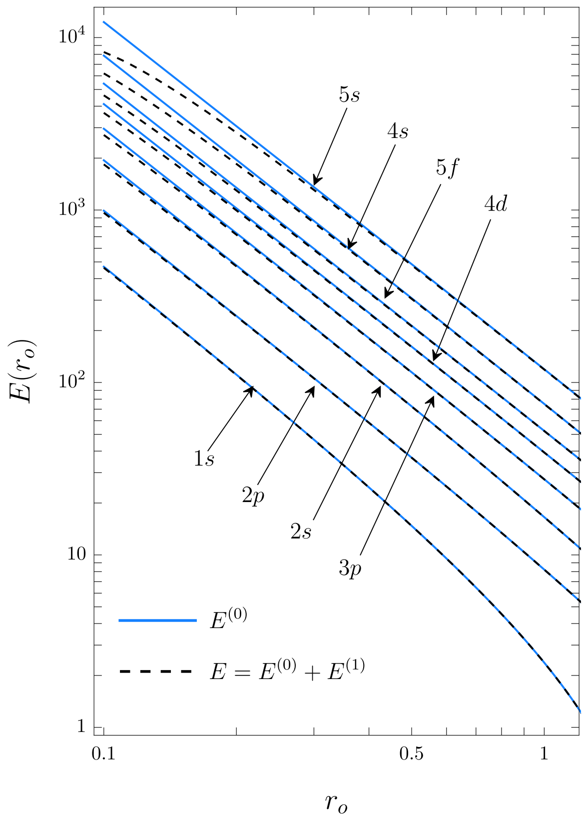

FIG. 12. Relativistic contribution to the energy of a confined H atom as a function of the cavity size r_o. Solid blue lines correspond to the expectation value of the unperturbed Hamiltonian, $\hat{H}^{(0)}$, while the dashed black lines to the perturbed Hamiltonian, $\hat{H}^{(0)} + \hat{H}'$.

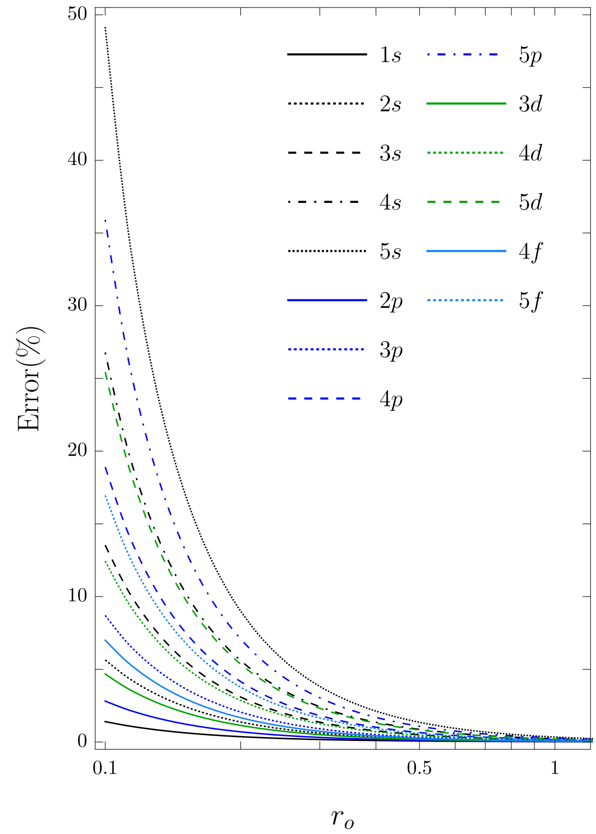

FIG. 13. Percentage error between the energies of the unperturbed-confined H atom, $E^{(0)}$, and the energy with the relativistic corrections, $E = E^{(0)} + E^{(1)}$, for the lowest $n < 6$ states.

contributions, we calculate the percentage error between the two energies by means of

$$\text{Error}(\%) = 100\frac{|E^{(1)}|}{|E^{(0)} + E^{(1)}|}. \tag{44}$$

The results obtained from Eq. (44) are shown in Fig. 13 as a function of r_o. From here, the percentage error increases monotonically as the cavity size decreases, and it is larger for excited states. For instance, at small radii $r_o = 0.1$, for nodeless states (solid lines) the difference goes from $\sim$1.4% to $\sim$7%, with the ground state (solid black line) being the one that has the smallest correction value to the energy, while the $4f$ state has a larger difference. These differences increase as ℓ does. States with one node (short-dashed lines) have corrections that go from $\sim$5.6%, for the $2s$ state, to $\sim$17%, for the $5f$ state. Therefore, the major difference corresponds to the $5s$ state, as observed in Figs. 12 and 13, which is expected, since the $5s$ state has more sudden changes on its kinetic energy as r_o decreases. It is worth mentioning that the relativistic correction for the energy of the $5s$ state is around 50%, making it necessary to consider higher-order corrections. Moreover, from Fig. 13 one notes that for radii $r_o > 1.1$ the relativistic corrections do not play an important role, since the percentage error in energy is less than 0.1%, for the states studied here. For this reason, we only report calculations for the interval $1 \leqslant r_o \leqslant 200$. These relativistic corrections provide a justification for the choice of the smallest cavity size for our study. These relativistic results are calculated by means of first-order perturbation theory, thus we expect that, by solving the Dirac equation, one will verify the validity of the first-order perturbation theory at these cavity sizes. Work is in progress along these lines.

IV. CONCLUSIONS

In this work, we have studied the position and momentum uncertainty inequalities and Heisenberg's uncertainty principle for the radial and vector representations. We analyze the behavior of the quadratic mean deviation for the electron position and momentum, as well as Heisenberg's uncertainty principle as a function of the cavity radius. Our results show the evolution from a free hydrogen atom at large cavity radii toward a free electron-in-a-box for small confinement. At small cavity radii, we find that the cavity overrides the Coulombic interaction. Thus, at small cavity sizes, the electron of the confined H atom behaves like a free particle in a spherical box. From the comparison of the results of a confined H atom and a particle-in-a-box, the domain regions of the Coulombic potential and kinetic energy are discerned clearly. These regions are characterized by the constant values of $\Delta\hat{r}\Delta\hat{p}_r$ and $\Delta\hat{\mathbf{r}}\Delta\hat{\mathbf{p}}$. Furthermore, the interval where this competition is relevant for each state of the confined atom is determined.

In the radial uncertainty approach, it is found that the compression breaks the coherence degree of the Rydberg states (pseudo-classical states) of the free system as it is exposed to extreme conditions of spatial limitations. The states increase their variance compared to the free system for the extremely confined case. In contrast to the radial representation, in the vector representation the most coherent state is the ground state of the confined atom, and it becomes more coherent as the cavity size decreases.

Moreover, in the vector representation and for large cavity sizes, it is found that the arrangement of $\Delta\hat{\mathbf{r}}$ is in bunches, which are determined by the principal quantum number n. However, as the system is compressed, these bunches suffer a degeneracy, as occurs in the case of $\langle r\rangle$, which degenerates as r_o decreases, showing just small differences with each other within the strong confinement regime. On the other hand, the degeneracy on the principal quantum number of the expectation values of the momentum (and energy) splits due to the compression of the system. This compensates the degeneracy of $\Delta\hat{\mathbf{r}}$ and gives rise to the behavior observed on the evolution of the uncertainty values $\Delta\hat{\mathbf{r}}\Delta\hat{\mathbf{p}}$ of each state of the system. In addition, the size of the cavity at which each excitation level is affected is determined by means of the $\Delta\hat{\mathbf{p}}$-crossing points between two consecutive states with the same symmetry. This has as a consequence that the changes in the electronic properties of the system are strongly related to the increments on the kinetic energy at these cavity sizes.

Finally, the region of validity for our nonrelativistic results is determined, finding that relativistic corrections are required for $r_o < 1.1$. Work is in progress to study this problem within the Dirac equation.

ACKNOWLEDGMENT

This work was supported in part by a scholarship to R.R.G. provided by CONAHCYT, with CVU No. 819058. We are also grateful for support from PAPIIT-UNAM IN-109-623 and LANCAD-UNAM-DGTIC-228 to R.C.T.

[1] E. Ley Koo, Rev. Mex. Fís. **64**, 326 (2018).
[2] G. H. Cocoletzi and W. L. Mochán, Surf. Sci. Rep. **57**, 1 (2005).
[3] K. D. Sen and K. Sen, *Electronic Structure of Quantum Confined Atoms and Molecules* (Springer, New York, 2014).
[4] W. Jaskólski, Phys. Rep. **271**, 1 (1996).
[5] V. Dolmatov, A. Baltenkov, J.-P. Connerade, and S. Manson, Radiat. Phys. Chem. **70**, 417 (2004).
[6] M. E. Madjet, H. S. Chakraborty, and S. T. Manson, Phys. Rev. Lett. **99**, 243003 (2007).
[7] Z. Kang Tang, Y. Nozue, and T. Goto, J. Phys. Soc. Jpn. **61**, 2943 (1992).
[8] O. Yeshchenko, I. Dmitruk, S. Koryakov, I. Pundyk, and Y. Barnakov, Solid State Commun. **133**, 109 (2005).
[9] H. Ullmaier, Nucl. Fusion **24**, 1039 (1984).
[10] A. J. Schwartz, M. A. Wall, T. G. Zocco, and W. G. Wolfer, Philos. Mag. **85**, 479 (2005).
[11] M. A. Martínez-Sánchez, C. Martínez-Flores, R. Vargas, J. Garza, R. Cabrera-Trujillo, and K. D. Sen, Phys. Rev. E **103**, 043202 (2021).
[12] C. Martínez-Flores and R. Cabrera-Trujillo, Eur. Phys. J. D **75**, 133 (2021).
[13] W. Lu and C. M. Lieber, J. Phys. D **39**, R387 (2006).
[14] M. Law, J. Goldberger, and P. Yang, Annu. Rev. Mater. Res. **34**, 83 (2004).
[15] M. A. Reed, Sci. Am. **268**, 118 (1993).
[16] M. Bacon, S. J. Bradley, and T. Nann, Part. Part. Syst. Charact. **31**, 415 (2014).
[17] X. Zheng, S.-Q. Ma, G.-F. Zhang, H. Fan, and W.-M. Liu, Sci. Rep. **10**, 150 (2020).
[18] W. Heisenberg, Z. Phys. **43**, 172 (1927).
[19] E. H. Kennard, Z. Phys. **44**, 326 (1927).
[20] H. P. Robertson, Phys. Rev. **34**, 163 (1929).
[21] D. Griffiths, *Introduction to Quantum Mechanics*, 3rd ed. (Cambridge University Press, Cambridge, 2017), pp. 105–109, 296–299.
[22] D. Bohm, *Quantum Theory*, Dover Books on Physics Series (Dover Publications, New York, 1951).
[23] S. Zozor, M. Portesi, and C. Vignat, Physica A **387**, 4800 (2008).
[24] Y. Xiao, Y. Yang, X. Wang, Q. Liu, and M. Gu, Phys. Rev. Lett. **130**, 240201 (2023).
[25] S. Patil and K. Sen, Phys. Lett. A **362**, 109 (2007).
[26] P. Sánchez-Moreno, R. González-Férez, and J. S. Dehesa, New J. Phys. **8**, 330 (2006).
[27] I. Białynicki-Birula and J. Mycielski, Commun. Math. Phys. **44**, 129 (1975).
[28] A. Rényi, in *Proceedings of the Fourth Berkeley Symposium on Mathematical Statistics and Probability, Volume 1: Contributions to the Theory of Statistics* (University of California, Oakland, 1961), Vol. 4, p. 547.
[29] J. S. Dehesa, Entropy **23**, 1339 (2021).
[30] C. R. Estañón, N. Aquino, D. Puertas-Centeno, and J. S. Dehesa, Int. J. Quantum Chem. **120**, e26192 (2020).
[31] C. R. Estañón, N. Aquino, D. Puertas-Centeno, and J. S. Dehesa, Int. J. Quantum Chem. **121**, e26424 (2021).
[32] C. R. Estañón, H. E. Montgomery Jr., J. C. Angulo, and N. Aquino, Int. J. Quantum Chem. **124**, e27358 (2024).
[33] S. Majumdar, N. Mukherjee, and A. K. Roy, Chem. Phys. Lett. **687**, 322 (2017).
[34] W. K. Wootters and W. H. Zurek, Nature (London) **299**, 802 (1982).
[35] D. Dieks, Phys. Lett. A **92**, 271 (1982).
[36] N. Gisin, G. Ribordy, W. Tittel, and H. Zbinden, Rev. Mod. Phys. **74**, 145 (2002).
[37] S. Pirandola, U. L. Andersen, L. Banchi, M. Berta, D. Bunandar, R. Colbeck, D. Englund, T. Gehring, C. Lupo, C. Ottaviani, J. L. Pereira, M. Razavi, J. S. Shaari, M. Tomamichel, V. C. Usenko, G. Vallone, P. Villoresi, and P. Wallden, Adv. Opt. Photon. **12**, 1012 (2020).
[38] R. Schwonnek, L. Dammeier, and R. F. Werner, Phys. Rev. Lett. **119**, 170404 (2017).
[39] H. F. Hofmann and S. Takeuchi, Phys. Rev. A **68**, 032103 (2003).
[40] S. Liu, L.-Z. Mu, and H. Fan, Phys. Rev. A **91**, 042133 (2015).

[41] O. Gühne, Phys. Rev. Lett. **92**, 117903 (2004).

[42] J. Ma, X. Wang, C. Sun, and F. Nori, Phys. Rep. **509**, 89 (2011).

[43] D. J. Wineland, J. J. Bollinger, W. M. Itano, and D. J. Heinzen, Phys. Rev. A **50**, 67 (1994).

[44] M. Kitagawa and M. Ueda, Phys. Rev. A **47**, 5138 (1993).

[45] V. Giovannetti, S. Lloyd, and L. Maccone, Phys. Rev. Lett. **96**, 010401 (2006).

[46] V. Giovannetti, S. Lloyd, and L. Maccone, Phys. Rev. Lett. **108**, 260405 (2012).

[47] R.-X. Chen, L.-T. Shen, and S.-B. Zheng, Phys. Rev. A **91**, 022326 (2015).

[48] A. Mari, A. Farace, N. Didier, V. Giovannetti, and R. Fazio, Phys. Rev. Lett. **111**, 103605 (2013).

[49] F. Bemani, A. Motazedifard, R. Roknizadeh, M. H. Naderi, and D. Vitali, Phys. Rev. A **96**, 023805 (2017).

[50] X. Zheng and G.-F. Zhang, Quantum Inf. Process. **16**, 1 (2017).

[51] S. Mal, T. Pramanik, and A. S. Majumdar, Phys. Rev. A **87**, 012105 (2013).

[52] S. Goldman and C. Joslin, J. Phys. Chem. **96**, 6021 (1992).

[53] J. M. Ferreyra and C. R. Proetto, Am. J. Phys. **81**, 860 (2013).

[54] P. A. M. Dirac and R. H. Fowler, Proc. R. Soc. London, Ser. A **113**, 621 (1927).

[55] D. Deutsch, Phys. Rev. Lett. **50**, 631 (1983).

[56] A. Khelashvili and T. Nadareishvili, Int. J. Mod. Phys. B **36**, 2250072 (2022).

[57] J. D. Hey, Am. J. Phys. **61**, 28 (1993).

[58] J. D. Hey, Am. J. Phys. **61**, 741 (1993).

[59] U. Roy, S. Ghosh, and K. Bhattacharya, Rev. Mex. Fís. E **54**, 160 (2008).

[60] A. Khelashvili and T. Nadareishvili, Phys. Part. Nuclei **52**, 155 (2021).

[61] A. Khelashvili and T. Nadareishvili, Phys. Part. Nuclei **51**, 107 (2020).

[62] J. S. Dehesa and D. Puertas-Centeno, J. Phys. B: At., Mol. Opt. Phys. **54**, 065006 (2021).

[63] R. Cabrera-Trujillo and S. A. Cruz, Phys. Rev. A **87**, 012502 (2013).

[64] Wolfram Research, Inc., Mathematica, Version 13.3, Champaign, IL (2023).

[65] S. De Groot and C. Ten Seldam, Physica **12**, 669 (1946).

[66] J. R. Nielsen, *The Correspondence Principle (1918–1923)* (Elsevier, New York, 2013).

[67] M. Abramowitz and I. A. Stegun, *Handbook of Mathematical Functions With Formulas, Graphs, and Mathematical Tables* (Dover Publications, Mineola, New York, 1965).

[68] E. Ley-Koo and S. Rubinstein, J. Chem. Phys. **71**, 351 (1979).

[69] R. Cabrera-Trujillo and O. Vendrell, Am. J. Phys. **88**, 1103 (2020).